Resource Utilization of Agricultural Residues: One-Step Preparation of Biochar Derived From Pennisetum Giganteum For Efficiently Removing Chromium From Water In A Wide pH Range

Yao Chen
Kunming University of Science and Technology
Ping Ning C
kunming university
Rongrong Miao
Kunming University of Science and Technology
Liang He (heliang@kust.edu.cn)
Kunming University of Science and Technology
Qingqing Guan
Kunming University of Science and Technology

Research Article

Keywords: Agricultural residues, H3PO4-treated biochar, pH range, Cr(VI), Selective adsorption

Posted Date: June 10th, 2021

DOI: https://doi.org/10.21203/rs.3.rs-555967/v1

Version of Record: A version of this preprint was published at Environmental Science and Pollution Research on July 23rd, 2021. See the published version at https://doi.org/10.1007/s11356-021-15388-y.

Resource utilization of agricultural residues: One-step preparation of biochar derived from *Pennisetum giganteum* for efficiently removing chromium from water in a wide pH range

Yao Chen [a, c], Ping Ning c* Rongrong Miao [a, c], Liang He [b*], Qingqing Guan [a*],

[a]Faculty of Civil Engineering and Mechanics, Kunming University of Science and Technology, Kunming, China

[b]Faculty of Chemical Engineering, Kunming University of Science and Technology, Kunming, Yunnan 650500, China

[c]Faculty of Environmental Science and Engineering, Kunming University of Science and Technology, Kunming, China

Abstract: Biochars derived from agricultural residues, *Pennisetum giganteum*, were prepared by a one-step activation method after impregnated with H_3PO_4. The effects of activation temperature and H_3PO_4 impregnation method on the structure and performance of biochar were investigated. Characterizations such as XPS, FTIR, and N_2 adsorption-desorption curves showed that the P-containing biochar prepared by one-step method had a large specific surface area, large pores, and abundant surface functional groups. And, C-P, O-P, C-O, and other groups participated in the adsorption and removal of Cr(VI). Moreover, the target adsorbent has a good effect on Cr removal in a wide range of pH (the removal rate was more than 55.92%, at pH$\leqslant$9). Interestingly, the changing trend of pH value in the reaction process under different initial pH values proved that the adsorbent itself could regulate the pH of the external

* Corresponding Author: Tel: +86 15687654177

Email ID: heliangkmust@163.com (Liang HE); 15545488@qq.com (Qingqing Guan); ningping1958@163.com

solution by providing acid groups, thus keeping the adsorption equilibrium solution in a narrow pH range. In addition, the target adsorbent had excellently selective adsorption capacity and good removal capacity (⩾77.4%) after five times of reuse. This work should permit for providing a convenient utilization of *Pennisetum giganteum* agricultural residues and confirmed that the biochar treated with H_3PO_4 can remove chromium in a wider pH range through self-regulation.

Keywords: Agricultural residues; H_3PO_4-treated biochar; pH range; Cr(VI); Selective adsorption

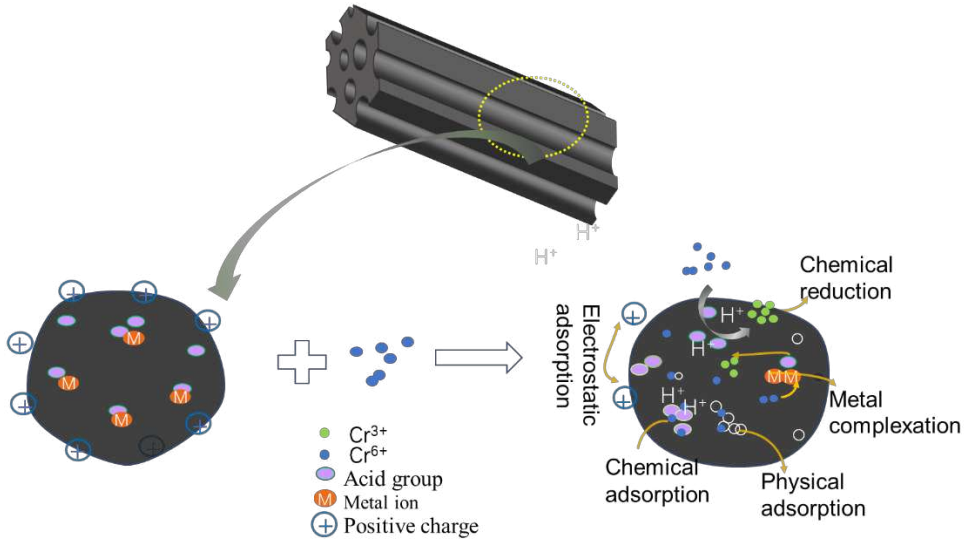

1. Introduction

Chromium (Cr) is a toxic heavy metal that constitutes a seriously threat to human health (Santiago et al. 2010). Chromium is derived from a wide range of sources, including electroplating, leather, printing and dyeing, metallurgy among others (Xin et al. 2018). In an aquatic environment, chromium primarily exists in two stable oxidation states: Cr (III) and Cr (VI). Cr (VI) has high mobility in the aquatic system and is about 500 times more toxic than Cr (III) (Jiang et al. 2015). Cr (VI) is carcinogenic (causing lung cancer), causes dermatitis, renal circulation, and other serious diseases. The US EPA regulated the Cr (VI) concentration standards as <0.1 mg L-1 for natural waters and

<0.05 mg L-1 of drinking water (Onchoke & Sasu 2016). Therefore, the treatment of Cr (VI) pollutants was of importance to public health and environmental protection.Several methods, including chemical precipitation, electrocoagulation, electrochemical treatment, reverse osmosis, membrane filtration or ion exchange and adsorption, have been employed to remove Cr (VI) from aqueous solutions(Ankur & Chandrajit 2016; Ramavandi et al. 2014; Zhao et al. 2017)**.** Among these methods, adsorption technique was considered as an efficient and attractive method owing to its effectiveness, simplicity, and cheapness (Jiang et al. 2018). At present, a variety of adsorbents(such as biochar, polymer, gel, natural, and waste) were reported to be used as clay minerals for the treatment of polluting wastewater (Sophia & Lima 2018). Biochar, is a relatively new adsorbent, that has attracted increasing attention on account of its rich and renewable properties in raw materials and the characteristics of "treating waste with waste" (Singh et al. 2019; Tong et al. 2019). Because of its rich surface functional groups, large porosity and ability to reduce reduce carbon emissions, biochar be used as a cheap carbon material adsorbent and can meet the requirements of low-cost adsorbent to remove heavy metals, and can be used to treat industrial wastewater. (Chao et al. 2015; Kong et al. 2014). The removal of metal ion by biochar is the result of a variety of mechanisms, including precipitation, complexation, ion exchange, electrostatic adsorption and physical adsorption (Dong et al. 2011a). Specific ligands and functional groups, such as -OH and -COOH on the surface of biochar can form complexes or precipitates with heavy metals (Mahdavi et al. 2013), which belonged to chemical adsorption. However, physical adsorption mainly depended on the surface properties of biochar, such as specific surface area and pore structure (Sigmund et al. 2017). Most studies showed that it was impossible to become an important mechanism for heavy

metal adsorption. The surface charge of biochar adsorbs metal ions with an opposite charge through electrostatic interaction, which is one of the main mechanisms of removing heavy metal ions by biochar. For example, biochar prepared at high temperature (>400 ℃) is easy to form a graphene structure, which further improves the electrostatic adsorption capacity of biochar and heavy metals (Wang 2018).

Generally, the adsorption mechanism of metal ions by biochar prepared by different activators is quite different. T The common activators are $ZnCl_2$, KOH, Na_2CO_3, H_3PO_4, etc. Yang et al. (Li et al. 2020). Researchers (Yu et al. 2020) used $FeCl_3$ and $ZnCl_2$ modified corn straw to remove Cr (VI), and its adsorption capacity could reach 138.89 mg g-1, but the solution environment had to be adjusted to pH = 2 . The addition of polyethyleneimine and phosphorus increased the number of active centers of the biochar from the oil tea shell, and the adsorption capacity reached 355 mg g-1 (Chen et al. 2018). For the materials reported in the literature, the pH value of the solution usually should be adjusted to acidic conditions (usually pH<3), which was confined within a narrow range (Sigmund et al. 2017; Xin et al. 2018). Therefore, the development of new biochar adsorbents with low cost and large pH range is still the sustainable goal of environmental remediation. However, in the past, studies focused on how to improve the adsorption capacity of the adsorbent (Ahmadi et al. 2016), and few researchers paid attention to how to modify the adsorbent to make the adsorbent have better chromium removal effect in a wide range of pH.

Herein, a new type of H_3PO_4-porous carbon was prepared by direct pyrolysis Pennisetum giganteum, w which was earlier impregnated with phosphoric acid.. Homogeneous carbonized biomass materials were prepared by one-step carbonization activation at a lower temperature. The adsorption isotherm and kinetic model were

analyzed and the stability of P-pg BC was tested. The results showed that phosphoric acid activated biochar can self-regulate the pH of the system. By providing protons, the pH of the initial solution was finally maintained in a narrow pH range. The purpose of this study is to synthesize biochar with sufficient surface acidity, which can remove chromium in a wide range of pH, to reveal the relationship between surface groups and adsorption properties of biochar. remove chromium in a wide range of pH, to reveal the relationship between surface groups and adsorption properties of biochar.

2. Material and method

2.1 Materials and Reagents

Pennisetum giganteum was kindly provided by Kunming Hengfa Technology Co., Ltd, Yunnan, China. Sodium hydroxide (NaOH), phosphoric acid (≥ 85.0%)，acetone (≥ 99.0%)，furfural (≥ 99.5%), sulfuric acid (≥ 98%), potassium dichromate (≥ 99.9%), and the other AR reagents were purchased from Shanghai McLean Biochemical Technology Co., Ltd. Deionized water was used to prepare all solutions and all the experimental steps. All chemicals used in this study were of commercially available analytical grade and used without further purification.

2.2 Preparation of activated carbon from *Pennisetum giganteum* (P-*pg*BC)

First of all, the *Pennisetum giganteum* stem should be washed and dried overnight in the oven. The dried *Pennisetum giganteum* was crushed with a grinder, screened through a 40-60 mesh sieve, and packed in plastic bags for standby (named as raw material). And then, there were two kinds of activation methods: one was that the raw materials were pre-carbonized, and then the pre-carbonized *c*arbon was mixed with a certain proportion of phosphoric acid (1:1,1:2,1:3), and then activated directly in the N_2 atmosphere at target temperature (labeled as Yp-*pg*BC-X ºC), the other was mix the raw

material with phosphoric acid in a certain proportion (1:1, 1:3), immersed it in an oven at 60 ºC for 24 h, and then activated it in N_2 atmosphere at target temperature (labeled as Zp-*pg*BC-X ºC). Among them, the condition of pre-carbonization refered to that carbonization in nitrogen atomosphere at 400 ºC for 2 h in a tube furnace.

he activation temperature was between 300 ºC and 500 ºC, the rate was 5K/min, and the time was 1 h. The materials prepared by the two methods were washed to neutral with deionized water and then dried in the oven overnight. Grind the dried materials and put them into plastic bags for standby. At this point, the adsorbent was ready.

2.3 Characterization

S_{BET} and pore size of Z_P-*pg*BC-400 ºC were completed by Brunauer-Emmett-Teller and Barrett-Joiner-Halenda method. The phase structure of Z_P-*pg*BC-400 ºC was obtained via an X-ray diffractometer (XRD, PANalytical). Surface element composition and element valence analysis also were examined by X-ray photoelectron spectroscopy (XPS, Thermo fisher Scientific K-Alpha$^+$). Fourier transforms infrared (FTIR) spectra were recorded on an FTIR Spectrophotometer in the range of 4000–500 cm^{-1} using KBr pellet. SEM and EDS were performed by field emission scanning electron microscope (Sigma model, Zeiss, Germany).

2.4 Batch Cr(VI) adsorption experiments

The typical adsorption process is as follows: 50 mL Cr(VI) solution (10-100 mg/L) and required weight of adsorbent (0.5-2.0 g/L) were added in a 150 ml conical flask for a batch experiment. Also, the effects of pH (1-9), contact time (0-24 h), and temperature (25, 40, and 55 ºC) on Cr (VI) adsorption efficiency were also studied. And all speeds of the reciprocating shaker were set to 160 rpm. The pH of the solution was adjusted with 0.1 M NaOH and 0.1M HCl. After 24 h, The concentration of remaining Cr(VI) anions

in the adsorption medium was determined at 540 nm using a double beam UVeVIS spectrophotometer after complexation with 1,5 diphenylcarbazide. To ensure the accuracy, reliability, and reproducibility of the data, all the batch experiments were carried out in triplicate for statistical purposes and the adsorption capacities were calculated by the following equation:

Adsorption efficiency % :

$$\eta = \frac{C_0 - C}{C_0} \times 100\% \quad (1)$$

Adsorption capacity:

$$q = \frac{(C_0 - C)}{m} \times V \quad (2)$$

Where C_0 and C (mg/L) are the initial and equilibrium concentrations of Cr(VI), m is the mass of absorbent (g), and V (L) is the volume of solution.

3. Results and Discussion

3.1 Optimization of Activation Conditions

Before the formal experiment, a large number of pre experiments were carried out, and the best adsorption materials were selected. Firstly, the carbon materials prepared by KOH two-step activation method reported by our research group were tested. It was found that it took long time for the adsorption to reach equilibrium, and the high removal efficiency could be only under acidic conditions(文献). Therefore, five kinds of carbon materials were prepared by using phosphoric acid as an activator and their removal effects were tested. And, the concentration of Cr(VI) was 50 mg/L, the reaction temperature was 25 °C, and the amount of adsorbent was 0.1 g. The chromium solution used was the natural pH value.

According to Table S1, the biochar prepared via one-step method has a good removal effect on Cr(VI), and the optimal mass ratio of carbon to phosphorus is 1:3. Next, the effects of activation temperature on the surface area, pore volume, and

161 removal efficiency of porous carbon materials were studied. The results of chromium
162 adsorption experiments of the adsorbents prepared at three different activation
163 temperatures at different pH were tested (Fig.1). Very clearly, biochar prepared at 400
164 ºC had the best effect, and the removal rate was more than 98% at the pH of natural
165 chromium solution (pH = 5.25), which was much milder than the acidic conditions
166 reported in the literature. As shown in Table S2, Zp-*pg*BC-400 ºC had the best removal
167 effect, and the adsorption capacity reached 30.52 mg/g. And, the N_2
168 adsorption-desorption behavior of the Zp-*pg*BC-400 ºC has been displayed in Fig. 2,
169 which concluded that it had an excellent specific surface area (749.9 m^2/g) with a pore
170 diameter of ~4.6 nm. It can be seen from Fig. 2, it had an obvious hysteresis loop,
171 which belonged to the type IV adsorption curve and was an obvious adsorption curve
172 of mesoporous adsorption materials. The nitrogen adsorption and desorption curves of
173 materials calcined at 300 ºC and 500 ºC are shown in Fig. S1. The results showed that
174 the specific surface area of the material calcined at 300 ºC and 500 ºC are 81.9 m/g and
175 1032.02 m^2/g, and the pore sizes are 10.41nm and 4.84 nm, respectively. The material
176 calcined at 300 ºC had the smallest specific surface area, least adsorption sites, which
177 explained the poorest performance of Zp-*pg*BC-300 ºC. Compared to 400 ºC, the
178 specific surface area increased at 500 ºC, but the adsorption performance decreased.
179 The decrease in the adsorption properties may be due to the decreases in the number of
180 oxygen-containing groups at high temperatures (Calisto et al. 2014). The BET data
181 were in good agreement with the experimental results (Fig. 1).

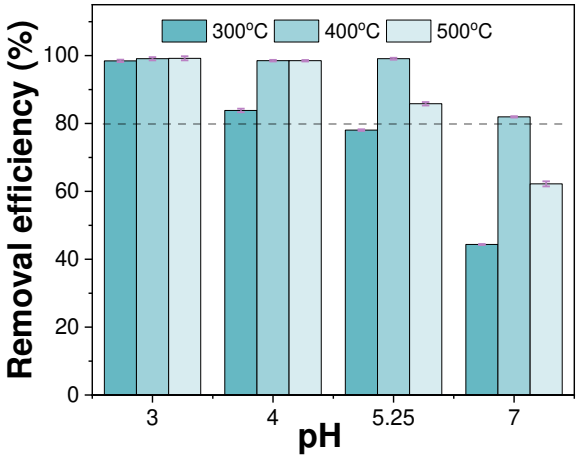

Fig. 1. Cr(VI) removal efficiency at three activation temperatures. (Initial concentrations = 50 mg/L, Solution pH 5.25, and T=25 °C).

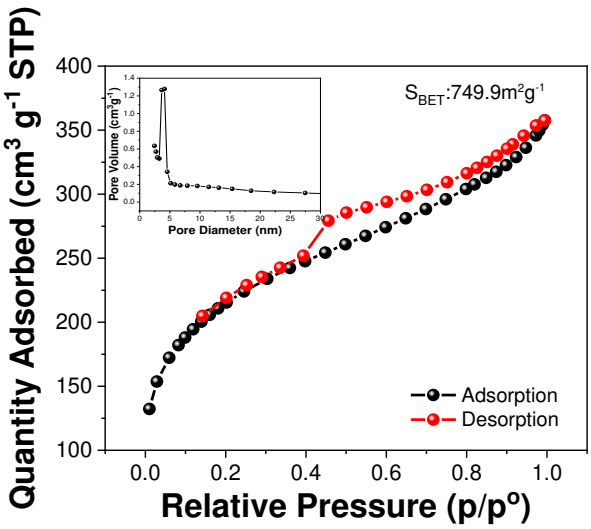

Fig. 2. N_2 adsorption/desorption isotherms and pore size distribution curve of Z_p-*pg*BC-400 °C.

3.2 Cr(VI) adsorption studies

3.2.1 Effect of adsorbent dosage and pH

Adsorbent dosage and the pH of Cr(VI) solution are of particular importance in analyzing the adsorption procedure and exploring the adsorption ability (Suganya & Kumar 2018; Zhang et al. 2017). In Fig. 3(a), removal of Cr(VI) was studied at 25 °C and 160 rpm for 24 h in the initial concentration of 50 mg/L, with different dosage of

adsorbents. With the increase of adsorbent concentration in solution, the removal efficiency of Cr first increased rapidly, then reached a good removal efficiency (> 97.01%) at the adding =1.5 g/L. Then with the increase of the amount of adsorbent, the adsorption capacity first tended to be stable and then decreased. Therefore, 1.5 g/L adsorbent can not only achieve a high removal rate but also achieve adsorption saturation.

The adsorption performance of biomass-based adsorbents may be closely related to the pH value of the solution, which affects both the existence of chromium and the charge properties of the adsorbent (Dong et al. 2011b; Yin et al. 2019; Zhang & Zheng 2015). As shown in Fig. 3(b), Cr(VI) had the maximum removal rate (> 97.01%) and higher adsorption capacity (31.4 mg/g) at pH ≤ 5.25. When the pH value is higher than 7, the removal rate and adsorption capacity decrease rapidly. At pH =7, the removal efficiency of Cr(VI) was 78.2%, and only 55.92% when it increased to 9. With the increase of pH value, the removal rate was decreasing, which was because the pH value of the solution greatly affected the existence form of chromium species (Zhang & Zheng 2015).

Interestingly, the removal effect of chromium was not bad at a high pH value. Therefore, Fig. 3(c) measures the real-time change of pH value during the adsorption process. It can be observed that when the initial pH was 7.04 and 8.98, the pH of the solution decreased rapidly within 10 minutes after the adsorbent was added. After 200 minutes, the pH of all solutions hardly changed and reached equilibrium. The mechanism analysis showed that the rich oxygen-containing functional groups on the surface of biochar could keep the pH value of the solution at 3.1 - 5.41, when the initial pH value was 3.04 - 8.98. The species distribution of chromium species at different pH

values is shown in Fig. 3d. Combined with Fig. 3c, it is found that the main chromium species in the solution is $HCrO_4^-$, in which the removal mechanism can be explained by Eq. 3. This was a good explanation of why Z_p-*pg*BC-400 ºC still had a good removal effect under alkaline conditions (See FTIR and XPS for more details).

$$HCrO_4^- + 7H^+ + 3e^- \longrightarrow Cr_3^+ + 4H_2O \quad (3)$$

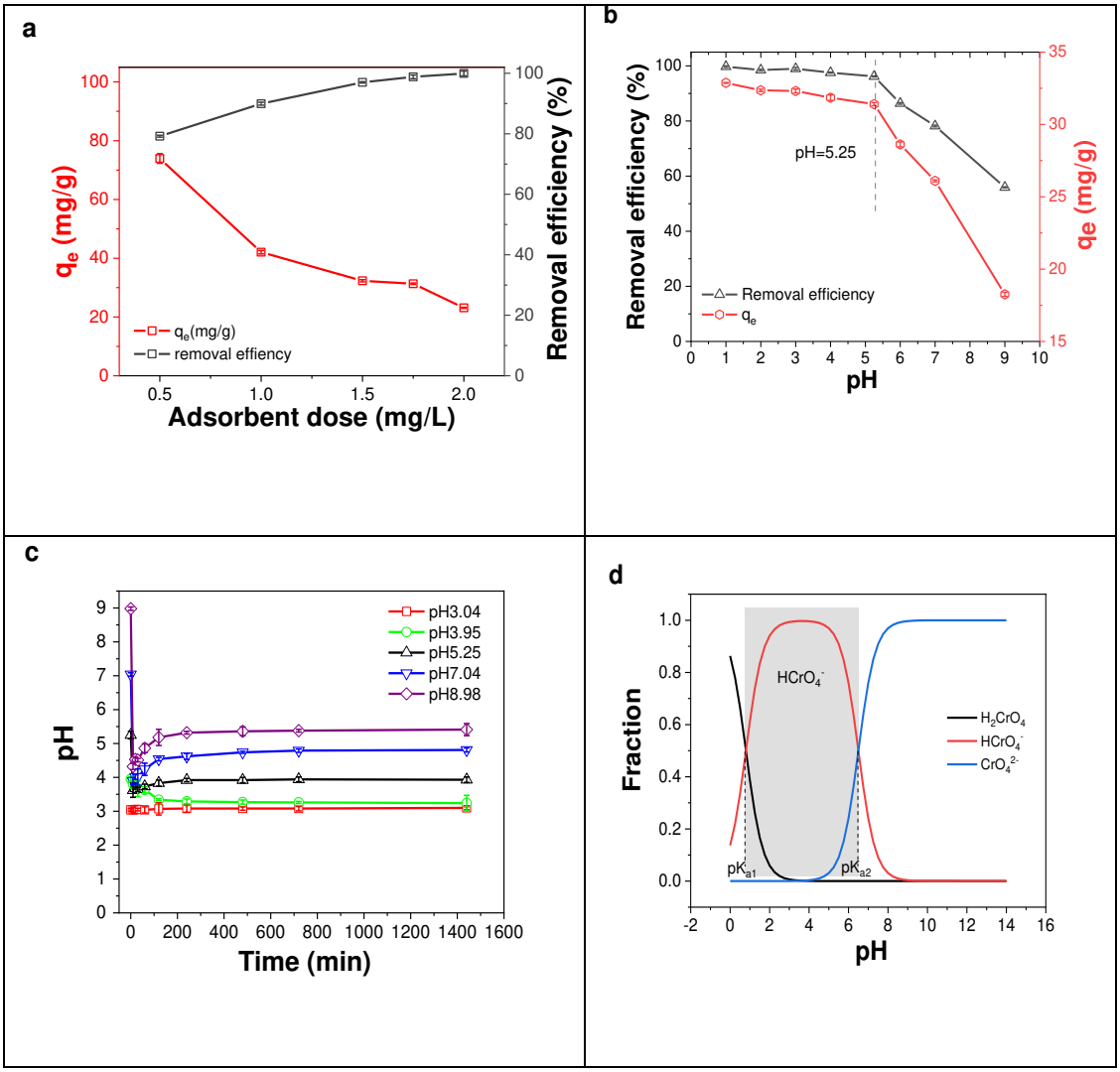

Fig. 3. Effect of dosage (a) and solution pH (b) on Cr(VI) removal; (c)pH changing trend during reaction under various initial pH (5.25 was the intrinsic pH of the solution). T=298 K, C_0(VI)=50 mg/g, rpm=160

3.2.2 Adsorption kinetics

Various factors affecting Cr(VI) adsorption, and the contact time is one of the most important factors. Therefore, To study the adsorption kinetics, the time dependence of the Cr(VI) adsorption capacity on the Z_P-*pg*BC had been investigated under optimum conditions. The four kinetics models were used to research the adsorption mechanisms: Pseudo-first order model (eq 4), Pseudo-second-order model (eq 5), Elovich model (eq 6), Intraparticle diffusion model (eq 7).

$$q_t = q_e(1 - e^{-k_1 t}) \quad (4)$$

$$q_t = \frac{k_2 q_e^2 t}{1 + k_2 q_e t} \quad (5)$$

$$q_t = A + BInt \quad (6)$$

$$q_t = k_i t^{1/2} + C \quad (7)$$

In Fig. 4(a), it was found that after 5 minutes, the removal amount of Cr(VI) reached 81.85%, and the adsorption capacity reached 26.84 mg/g, then gradually flat after 480 min. In Fig. 4(a) it can be known that the R-square value (R^2) of pseudo-second-order (R^2 = 0.999) was a little higher than that of the pseudo-first-order (R^2 = 0.946), which indicated that the rate-limiting step was a chemisorption process (Liang et al. 2020). Besides, the adsorption values calculated by the pseudo-second adsorption kinetic models (q_2 = 32.05128 mg/g) were closed to the experimental data (32.458 mg/g). In Fig. 4(b), the results exhibited that the adsorption efficiency can be well fitted with the Elovich model with R^2 of = 0.9956, suggesting the existence of the chemical effect, and Cr(VI) adsorption was on the surface of heterogeneous solid adsorption (Guan et al. 2020). In Fig. 4 (c), R^2 of the three-stage intraparticle diffusion model were greater than 0.99, indicating that the internal diffusion played a certain role in the actual adsorption process, but the lines have not been passed through the origin,

exhibiting that intragranular diffusion is not a speed limiting step.

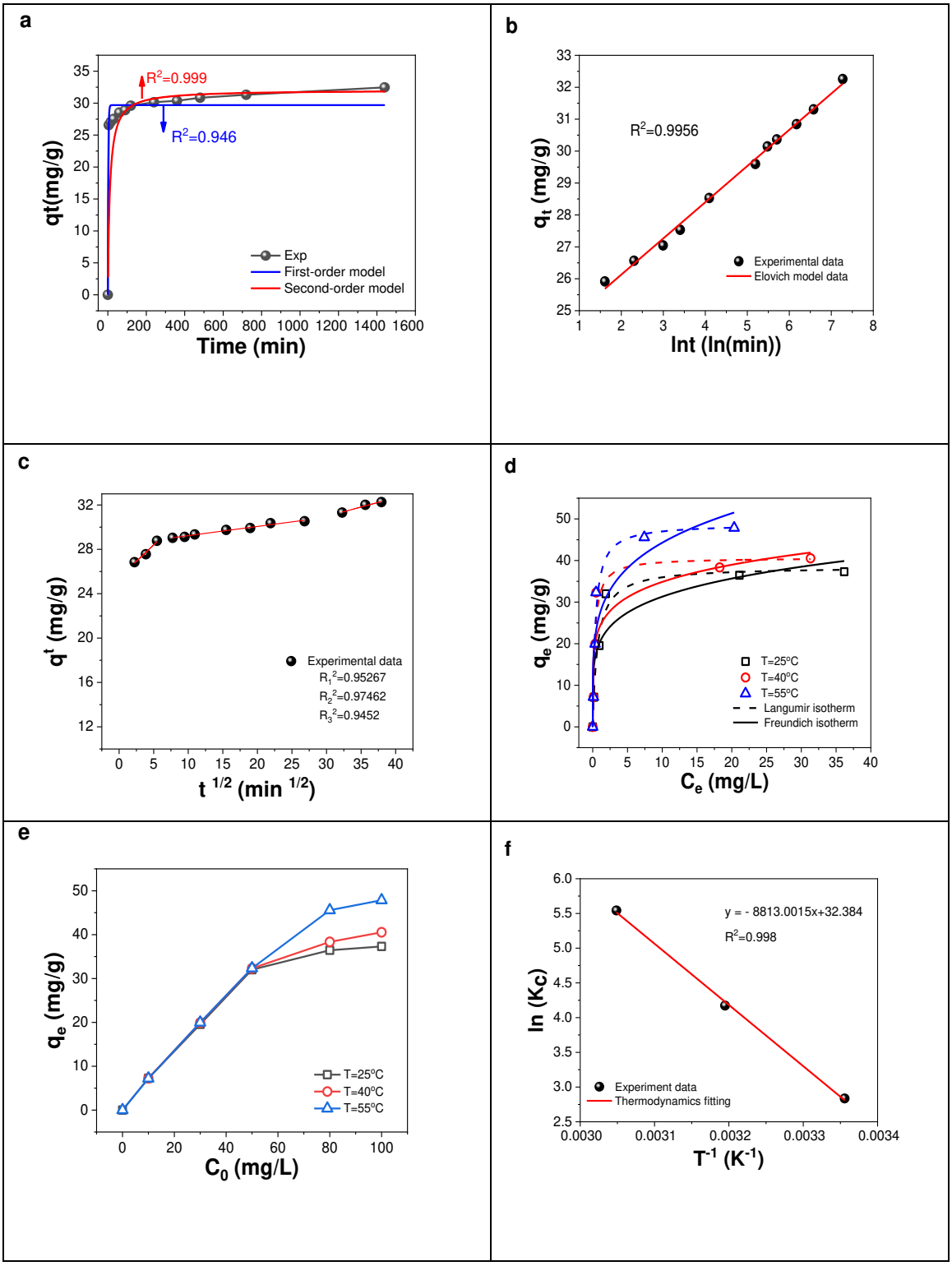

Fig. 4. (a) Pseudo-first order and and Pesudo-second order; (b) Elovich model; (c) Intra-partice diffusion kinetic model; (d) Langmuir and Freundich adsorption isotherms; (e) Effects of original concentration on adsorption capacity at different temperature;(f)

Thermodynamic plot solution pH 5.25, mass of adsorbent=1.5 g/L, and T=25 ºC).

3.2.3 Adsorption Isotherms

Two well-known adsorption isotherm models, Langmuir and Freundlich isotherm models, are commonly used to describe the adsorption process (Petkovska & Menka 2014). The equilibrium adsorption isotherms were investigated at three temperatures (25, 40, and 55 ºC) with different initial concentrations of Cr(VI). The relevant parameters results were shown in Table S3 corresponding equations of Langmuir and Freundlich isotherms are represented as follows:

Langmuir model: $q_e = \mathrm{K}QCe/(1 + \mathrm{K}Ce)$ (8)

Freundlich model: $\mathrm{q}_e = \mathrm{K}_F\mathrm{C}_e^n$ (9)

Where q_e (mg/g) is the equilibrium adsorption of Cr(VI) (mg/g), C_e (mg/L) is the equilibrium concentration in solution; q_{max} (mg/g) is the monolayer capacity of the adsorbent; K_L is the Langmuir constant related to the free energy of adsorption; K_F and n are the Freundlich constant and the heterogeneity factor, respectively.

In Fig. 4(d), It was obvious that the Langmuir model fitted the experimental data better. According to Table S3, the correlation coefficient (R^2), compared with the Freundlich model, the Langmuir model at three different temperatures showed a better fitting (R^2>0.95), which indicated that the adsorption process could be explained via the Langmuir model, can reflect that both physical and chemical adsorption are involved in the adsorption process and the maximum adsorption capacity was about 48.813 mg/g at 333 K. The results showed that the adsorption of Cr (VI) on the adsorbent was not caused by a single factor, but affected by a variety of adsorption processes.

3.2.4 Thermodynamic study

Thermodynamic study can reveal the feasibility and spontaneous nature of the adsorption process. Thermodynamic parameters are shown in Fig. S3. and Fig. 1. As shown in Fig. 4(e), with the increases in temperature, the adsorption capacity increased from 7.12 to 47.85 mg/g that higher temperature was beneficial to the adsorption process. When the initial concentration was more than 50 mg/L, the temperature has a significant effect on the removal of Cr(VI). To further explore the effect of temperature on adsorption efficiency, the thermodynamic parameters are determined using the following equations:

$$\Delta G = -RTlnk_c \quad (10)$$

$$lnk_c = \frac{\Delta S}{R} - \frac{\Delta H}{RT} \quad (11)$$

$$k_c = \frac{q_e}{c_e} \quad (12)$$

Tabel 1. Thermodynamic parameters at different temperatures

T(K)	Lnk_c	ΔG(kJ/mol)	ΔH(kJ/mol)	ΔS(J/(mol.K))	R^2
298	2.835812	-7.02593	73.27	269.2406	0.998
313	4.173052	-10.339			
328	5.543335	-13.734			

Where q_e and C_e are equilibration adsorption amount and equilibration adsorbate concentration, R (8.314 J /mol/k) is the universal gas constant, K_c is the distribution coefficient at each temperature (mg/L) and T is the absolute temperature. Enthalpy changes (ΔH), entropy changes (ΔS), free Gibbs energy (ΔG) are three basic thermodynamics parameters associated with the adsorption process.

Thermodynamic constants and curves have shown in Fig. 4(e) and (f) and Table 1, respectively. When the initial concentration was greater than 50mg/L, the temperature

299 in increases significantly increased the adsorption capacity (Fig. 4(e)), and the linear
300 fitted well between LnK_0 and 1/T (Fig. 4(f)) And usually, $\Delta H > 0$ indicated that the
301 reaction was an endothermic process. The positive ΔH value of 73.27 kJ/mol (Tabel 1)
302 indicated the adsorption of Cr(VI) was an endothermic process (Chen et al. 2011). It
303 should be noted that ΔH is generally in the range of 2.1-20.9 KJ/mol, which belongs to
304 physical adsorption, while the chemical interaction involving complexation is usually
305 between 20.9 - 418.4 KJ/mol (Rathinam et al. 2014). Therefore, the thermodynamic
306 parameters well proved that the adsorption process in this study was a chemical
307 adsorption process involving complexation. Besides, the positive $\Delta S > 0$ (296.2406
308 J/mol/K) represented increasing in reaction system disorder, which was favorable to
309 the adsorption reaction. And, $\Delta G < 0$ manifested Cr(VI) adsorption on Z_p-*pg*BC was a
310 spontaneous reaction (Liu & Xu 2007). The ΔG values decreased when the
311 temperature increased, which indicated that the spontaneous degree also increased with
312 the temperature increasing.
313 3.2.5 Evaluation of selective adsorption
314 To investigate the selective properties of the Z_p-*pg*BC-400 ºC, adsorption of
315 Cr(VI) in the presence of competitive ions in the binary system have been studied.
316 Because Cr(VI) existed in the form of the anion in solution, only the influence of anion
317 on its selective adsorption was studied. The concentration of Cr(VI) in all solutions
318 was 50 mg/L. In Fig. 5, it can be seen that the removal efficiency of Cr(VI) was close
319 to 100% (except CO_3^{2-}) when the concentration of co-existing ions increases from 30
320 mg/L to 100 mg/L. To explore whether there was competitive adsorption between
321 CO_3^{2-} and Cr, or whether the addition of CO_3^{2-} changed the inherent pH value of the
322 solution, the pH value of the solution with CO_3^{2-} added was determined. The pH values

of 30, 50, 100 mg/L carbonate solution and the Cr ion coexistence solution were 6.26, 7.62, and 10.12, respectively. When the pH value of the solution added with carbonate was adjusted to about 5.20, the Cr(VI) removal rate was restored to nearly 100%. The reason was that the addition of carbonate changed the pH value of the solution, exceeding the pH window, resulting in a decrease in the adsorption effect. Therefore, the results indicated that the prepared Z_p-*pg*BC-400 ºC had high selectivity towards Cr(VI) in the presence of competitive ions, and it can recognize $Cr_2O_7^{2-}$ very well even in the presence of interfering ions to a quite high extent.

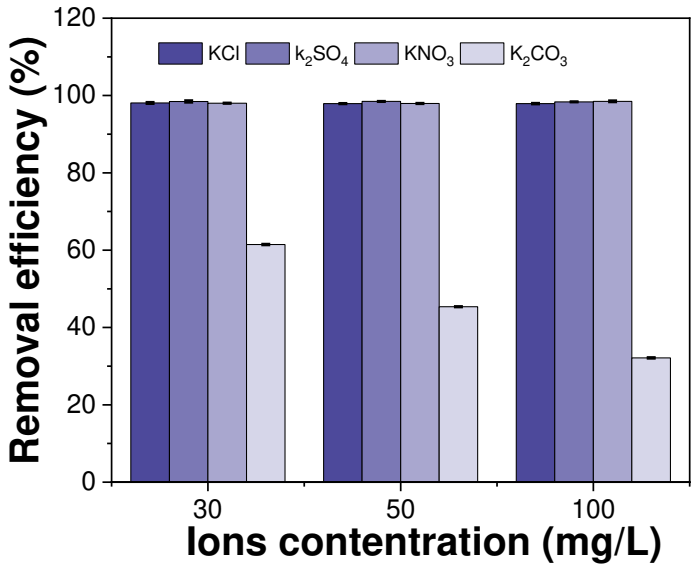

Fig. 5. Effect of four common co-existing ions on Cr(VI) removal efficiency

3.3 Characteristics and mechanism

3.3.1 XRD and FTIR analysis

Fig. 6(a) showed the XRD pattern of the adsorbed material. The strong broad peaks at 23° and 44° correspond to the crystal planes of (002) and (100) representing the typical graphitic carbon, which is often observed for pyrolyzed biomass carbons (Liu et al. 2014). Fig. 6(b) showed the infrared spectra before and after adsorption, on the whole, the positions of functional groups were almost unchanged before and after

adsorption, which may be the reason why the adsorbent can be removed efficiently after several times of adsorption and desorption. Functional groups in biochar are -OH (3000-3500 cm^{-1}), C=O/C-O-C (1680 cm^{-1}), $-CH_2$ (2932, 2856 cm^{-1}), etc. The characteristic absorption bands at 2932cm^{-1} and 2856cm^{-1} belong to methylene stretching and bending vibrations (Chaofan et al. 2018). The characteristic peaks at 1680 and 1570 cm^{-1} were attributed to the stretching vibrations of C=C/C=O/C-O-C respectively due to generated polar functional groups on the Z_p-*pg*BC-400 ºC after acid functionalization. And, the peak at 1134, 1057 cm^{-1} could be assigned to P-O/P=O groups (Chen et al. 2018). At peaks of 898 cm^{-1} and 804 cm^{-1}, new substances were formed, which could be the vibration of Cr-O (Li et al. 2009). The FTIR results indicated that the adsorbent contained kinds of functional groups, such as -COOH, C=O, -OH, P=O/P-O, and R-C-O-C, which could provide numerous actives sites.

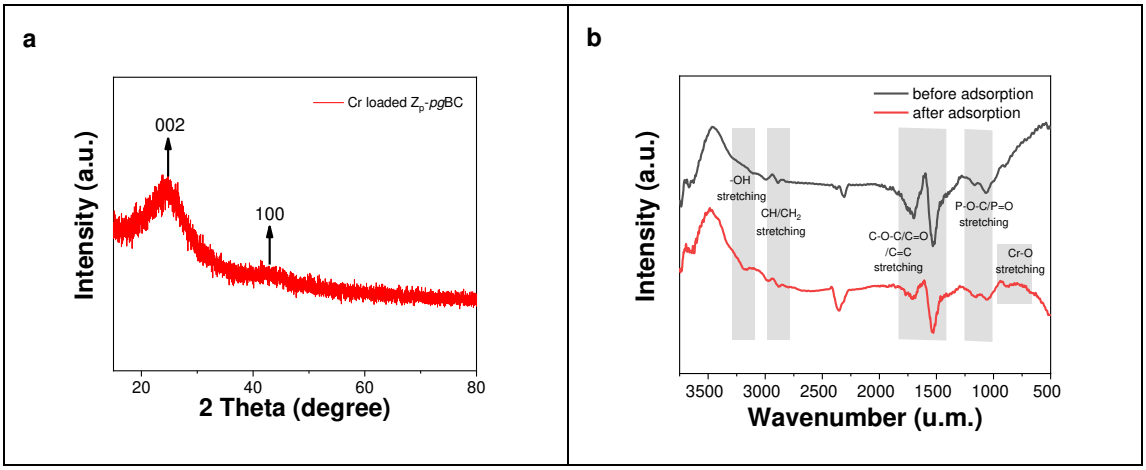

Fig. 6. (a) XRD patterns, (b) FTIR spectra of Z_p-*pg*BC-400ºC.

3.3.2 Structure and Morphology analysis

SEM is widely used to study the morphological and surface characteristics of the adsorbent materials. The surface morphological of raw materials (*Pennisetum giganteum*) and Z_p-*pg*BC-400 ºC before and after adsorption are shown in Fig. 7. It can be observed that Fig. 7(a) presented a compact structure with low porosity and a

smooth surface. However, after mixed with phosphoric acid impregnation (Fig. 7(b) and Fig. 7(c)), the surface looked very rough with irregular cavities structure. This structural change may be due to the addition of phosphoric acid, a large number of irregular groups were introduced. From adsorption, this structure is conducive to adsorption. Moreover, for the difference between Fig. 7(c) and (b), which may be the result of the reaction between Cr and oxygen-containing functional groups on carbon materials. The rich distribution of C, O, and P elemental indicates the existence of a large number of oxygen-containing functional groups and Phosphorus oxygen functional groups on the Zp-*pg*BC-400 ºC surface. Besides, the uniform distribution of chromium in Fig. 7(g) indicated that Cr(VI) was successfully adsorbed on the surface of Z_p-*pg*BC-400 ºC. The EDS mapping analysis results of Z_p-*pg*BC-400 ºC after adsorbing of Cr(VI) have been described in Fig. 7(d-g). Mapping results showed that that Cr(VI) contaminants have been homogeneously distributed. And the element content in Fig. 7(i). The prepared carbon materials have a large specific surface area (749.9 m^2/g), large pore volume, rod-like porous structure, abundant P atoms, and abundant oxygen-containing functional groups.

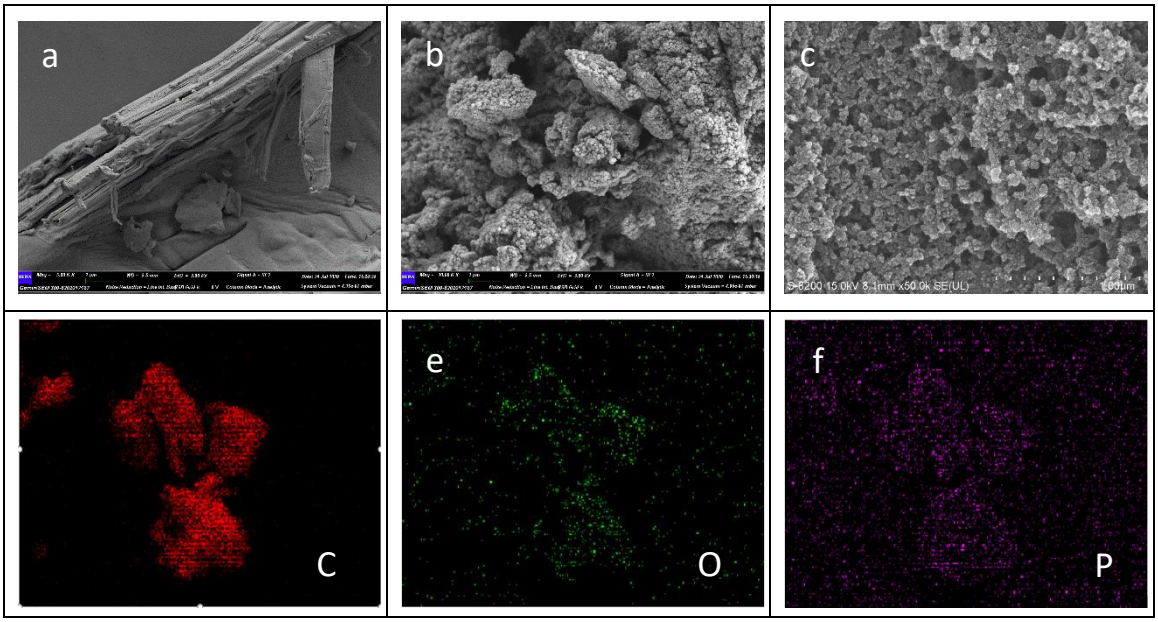

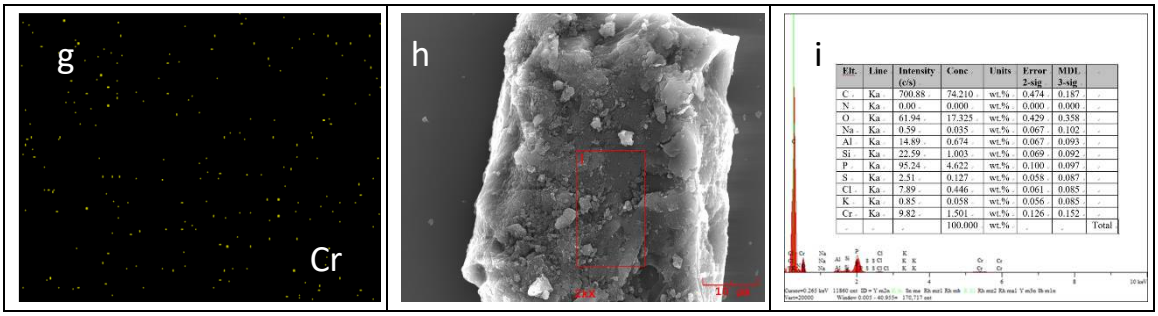

Elt.	Line	Intensity (c/s)	Conc	Units	Error 2-sig	MDL 3-sig	
C	Ka	700.88	74.210	wt.%	0.474	0.187	
N	Ka	0.00	0.000	wt.%	0.000	0.000	
O	Ka	61.94	17.325	wt.%	0.429	0.358	
Na	Ka	0.59	0.035	wt.%	0.067	0.102	
Al	Ka	14.89	0.674	wt.%	0.067	0.093	
Si	Ka	22.59	1.003	wt.%	0.069	0.092	
P	Ka	95.24	4.622	wt.%	0.100	0.097	
S	Ka	2.51	0.127	wt.%	0.058	0.087	
Cl	Ka	7.89	0.446	wt.%	0.061	0.085	
K	Ka	0.85	0.058	wt.%	0.056	0.085	
Cr	Ka	9.82	1.501	wt.%	0.126	0.152	
			100.000	wt.%			Total

Fig. 7 SEM images of *Pennisetum giganteum* (a); Z_p-*pg*BC-400 ºC before (b) and after (c) Cr adsorption; Elemental mapping of (d) C, (e) O, (f) P, (g) Cr; (h) EDS point scan analysis area and (j) the corresponding EDS patterns.

3.3.3 XPS and morphology analysis

Besides element composition, XPS can also provide information on their valences of adsorbent and adsorbed species. The fine spectrum of C_{1s} (Fig. 8 (a)) can be fitted to 3 peaks centered on the binding energies of about ~284.6 eV, ~286.0 eV, and ~289.4 eV, corresponding to the presence of C-C, C-O/C-P, and C=O bonds, respectively (Chen et al. 2018). The binding energy position and relative content of carbon changed little before and after use, indicating that the chemical state of the C element in biochar is relatively stable. Three peaks at about ~530 eV, ~532 eV, and ~534 eV in Fig.8(b) represented of C=O/P=O, C-O/P-O, and -OH/H_2O (Chen et al. 2020; Li et al. 2020). And, the O elements in the adsorption after also could observe three peaks. It is worth noting that the content of C-O/P-O (~532 eV) decreased, which indicated that the C-O/P-O bond was oxidized to C=O/P=O during the reaction (Xu et al. 2019a; Zhou et al. 2016b). And the binding energy of O shifted positively after the reaction, which indicated that the electron cloud density of O decreased, resulting in the detection of a higher binding energy band. In the process of Cr (VI) reduction, the O atom was the electron donor (Gao et al. 2013). This indicated that C-O/P-O participates in the adsorption and reduction of Cr(VI). Also, the fine spectrum of P_{2p} has been changed

394 significantly. Attentively, for the phosphorus species, the strength of Z_p-*pg*BC-400 ºC
395 decreased significantly after adsorption. And, the proportion of C-P decreased while
396 C-P=O increased. The increase of C-P=O content indicated that after adsorption of Cr
397 on biochar, the C-P bond of biochar was broken and the P=O bond was formed with
398 chromate to form chromium phosphate. After adsorption, a new peak of $CrPO_4$
399 appeared at the binding energy of 133.4 eV (Fig. 8 (c)), which indicated that the
400 P-containing group can interact and precipitate with some Cr (VI) ions. The fine
401 spectra of Cr(VI) are shown in Fig. 8(d). Binding energies at 578.06 eV and 587.47 eV
402 were assigned to Cr $2P_{3/2}$ and $2P_{1/2}$ orbitals of Cr(Ⅲ), respectively (Xu et al. 2019b;
403 Zhou et al. 2016a). The small peak at 582.21 eV was unreduced hexavalent chromium.
404 Finally, in Fig. S2, the strength of C_{1s}/O_{1s}/P_{2P} decreased after adsorption can be
405 observed, and Cr_{2p} appeared near 577 eV, further indicating that Cr was successfully
406 adsorbed on the surface of biochar during the adsorption process.

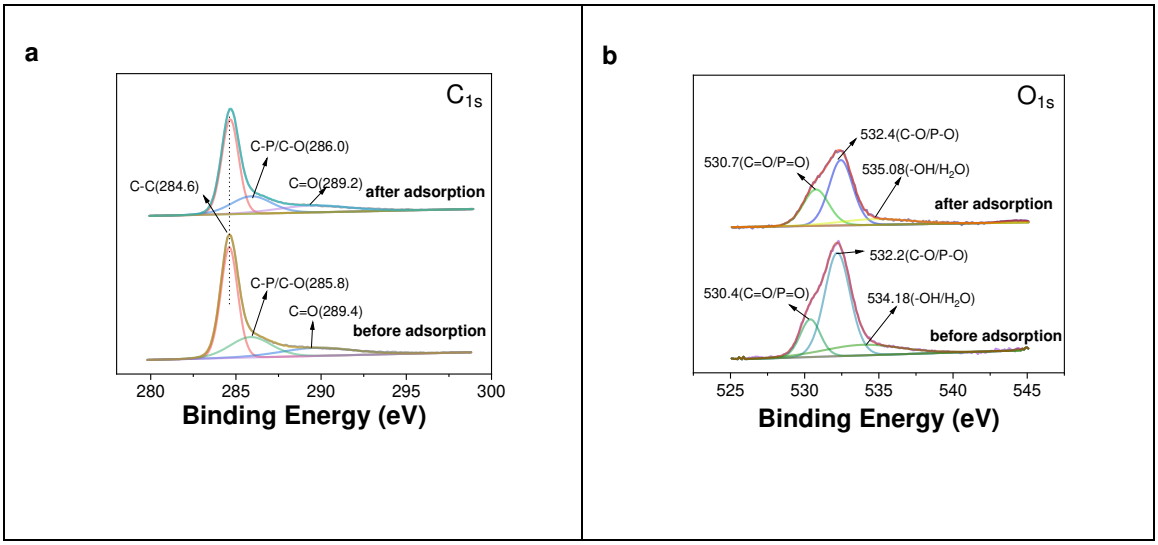

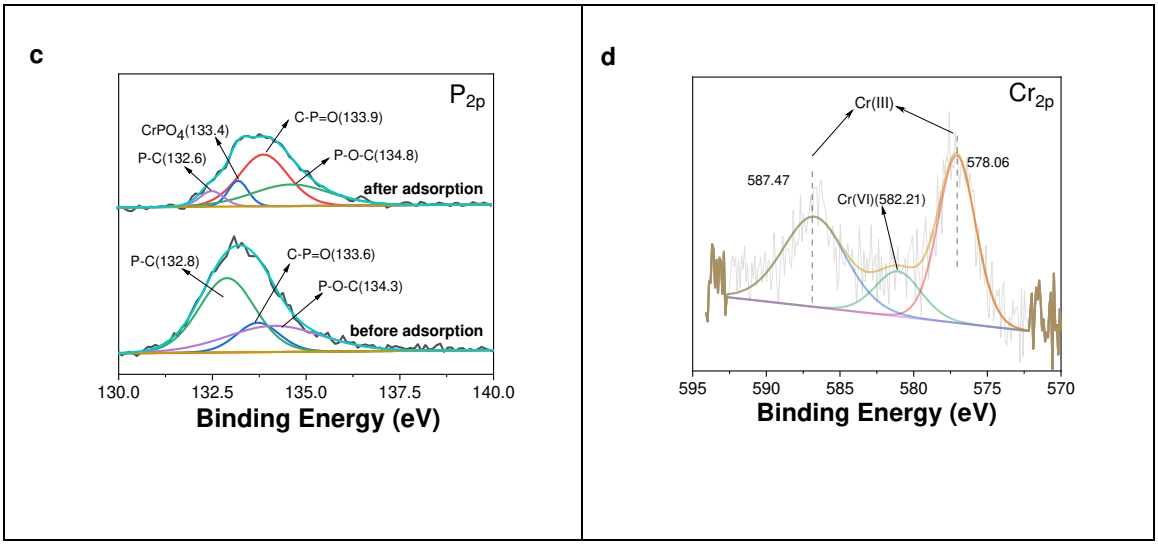

Fig. 8. XPS spectrum of Zp-*pg*BC-400 ºC before and after Cr(VI) adsorption. (a) C_{1s}, (b) O_{1s} and (c) P_{2p} and (d) Cr_{2p}.

3.3.4 Regeneration and adsorption/reduction mechanism

To investigate the reusability and stability of synthesized adsorbent, five times adsorption-desorption cycles were performed under the optimal conditions mentioned above. The details were as follows: before reusing, the used adsorbent should be filtered, then immersed in 0.1 M NaOH solution, stirred for 24 h, and then filtered and dried overnight in an oven at 80 ºC. The results of five cycles were shown in Fig. 9. The removal efficiency of Cr(VI) decreased from 99.03% to 77.74% after cycles five times. After the fifth cycle, the Cr removal efficiency was more than 77%, which indicated that the synthesized adsorbent can be used many times without a significant decrease in adsorption capacity. This was much better than the stability after four uses reported by our research team (less than 70%) (Guan et al. 2020).

The results showed that Cr(VI) can be removed by the adsorption/reduction process in a wide range of operating pH. Based on the above analysis, the adsorption mechanism was proposed and systematically investigated (Fig. 10). There were many acidic groups on the surface of Zp-*pg*BC-400 ºC, such as phosphate, carboxyl, carbonyl,

and so on. These acidic groups can release protons to maintain pH in a relatively narrow range when the external environment solution pH is relatively high. This can explain that the adsorbent can reach more than half of the removal rate under alkaline conditions. To sum up, the removal mechanism was shown in Fig.10, including (1) electrostatic attraction; (2) physical adsorption in porous structures; (3) chemical reduction and adsorption, the most main adsorption process; and (5) metal complexation. The combined action of various functions is the reason why the adsorbent can effectively remove Cr(VI).

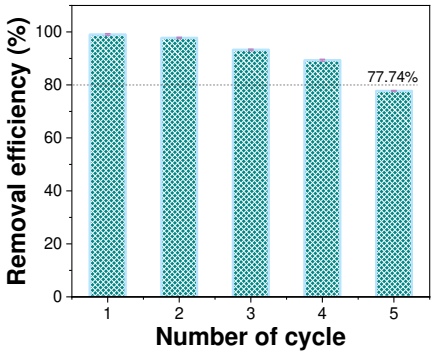

Fig. 9. Cycle times of Z_p-*pg*BC-400 ºC on Cr(VI) removal efficiency

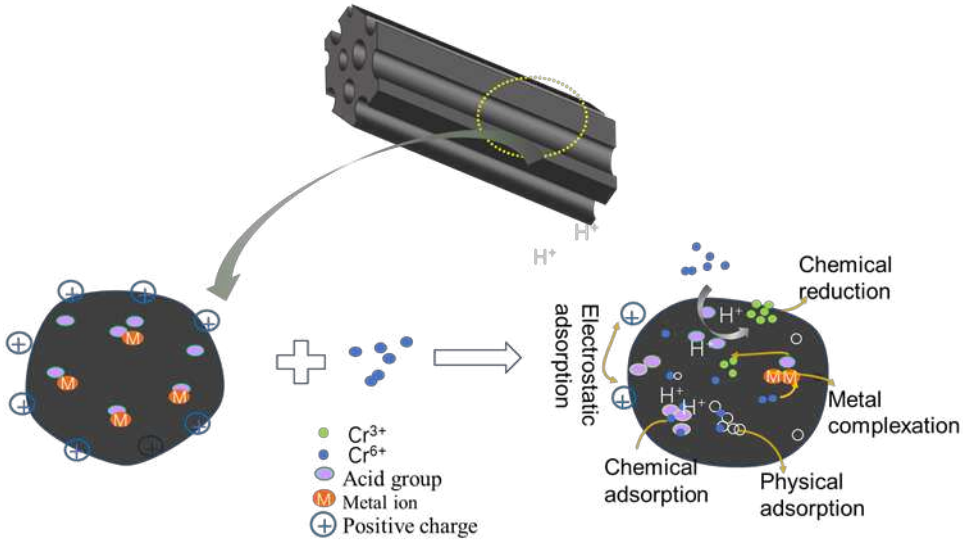

Fig. 10. Schematic illustration of Cr(VI) removal mechanism

4. Conclusion

In this paper, biochar with enough acidic surface groups was synthesized, which

maintained the pH value of the system in a relatively stable range during the adsorption process. Cr(VI) uptake experiments displayed that in a wide pH range (1-6), the removal rate of Cr(VI) in water by biochar is as high as 86.39%. The mechanism analysis showed that the rich oxygen-containing functional groups on the surface of biochar could keep the pH value of the solution at 3.1-5.41 when the initial pH value was 3.04 - 8.98. The maximum adsorption capacity can reach 48.813 mg/g, and it is accorded with pseudo-second-order kinetics and L-type adsorption model. The results of five times adsorption-desorption experiments showed that the activated biochar directly impregnated with phosphoric acid had good stability. This work provided an effective solution for the removal of chromium in the pH range of a large window and opened up a new way for the resource utilization of *Pennisetum giganteum*, a common agricultural and forestry waste.

Ethical Approval

Not applicable

Consent to Participate

Not applicable

Consent to Publish

Consent

Authors Contributions

Chenyao : Conceptualization, Validation, Formal analysis, Data curation, writing original draft. Ningping: Supervision, Project administration, Funding acquisition.Miaorongrong: Draft modification.Heliang: Investigation, Methodology, Writing-review & editing.Guanqingqing: Supervision, Project administration, Funding

462 acquisition.

463 **Funding**

464 This work is co-supported by the National Natural Science Foundation of China
465 (Grant No. 21968014) , the Analysis and Testing Foundation of Kunming University of
466 Science and Technology (No.2019M2018220705) ， and the National Key Research
467 and Development Program of China (Grant No. 2018YFC1902105, 2018YFC1902102,
468 and 2018YFC1902101).

469 **Competing Interests**

470 The authors declare that they have no known competing financial interests or
471 personal relationships that could have appeared to influence the work reported in this
472 paper.

473 **Availability of data and materials**

474 The datasets used and/or analysed during the current study are available from the
475 corresponding author on reasonable request.

476 All data generated or analysed during this study are included in this published
477 article [and its supplementary information files].

478 **References**

479 Ahmadi, M., Kouhgardi, E., Ramavandi, B. 2016. Physico-chemical study of dew
480 melon peel biochar for chromium attenuation from simulated and actual wastewaters.
481 *Korean Journal of Chemical Engineering*, **33**(9), 2589-2601.

482 Ankur, G., Chandrajit, B. 2016. Simultaneous Adsorption of Cr(VI) and Phenol from
483 Binary Mixture Using Iron Incorporated Rice Husk: Insight to Multicomponent
484 Equilibrium Isotherm. *International Journal of Chemical Engineering,2016,(2016-3-7)*,
485 **2016**, 1-11.

Calisto, V., Ferreira, C.I., Santos, S.M., Gil, M.V., Otero, M., Esteves, V.I. 2014. Production of adsorbents by pyrolysis of paper mill sludge and application on the removal of citalopram from water. *Bioresour Technol*, **166**, 335-44.

Chao, G., Liu, Y., Tan, X., Wang, S., Zeng, G., Zheng, B., Li, T., Jiang, Z., Wei, L. 2015. Effect of porous zinc–biochar nanocomposites on Cr(VI) adsorption from aqueous solution. *Rsc Advances*, **5**.

Chaofan, Z., Huaili, Z., Yongjuan, W., Yili, W., Wenqi, Q., Qiang, A., Yongzhi, L. 2018. Synthesis of novel modified magnetic chitosan particles and their adsorption performance toward Cr(VI). *Bioresource Technology*, **267**, S0960852418309118-.

Chen, M., He, F., Hu, D., Bao, C., Huang, Q. 2020. Broadened operating pH range for adsorption/reduction of aqueous Cr(VI) using biochar from directly treated jute (Corchorus capsularis L.) fibers by H3PO4. *Chemical Engineering Journal*, **381**.

Chen, S., Wang, J., Wu, Z., Deng, Q., Tu, W., Dai, G., Zeng, Z., Deng, S. 2018. Enhanced Cr(VI) removal by polyethylenimine- and phosphorus-codoped hierarchical porous carbons. *Journal of Colloid and Interface Science*, **523**, 110-120.

Chen, S., Yue, Q., Gao, B., Qian, L., Xing, X. 2011. Removal of Cr(VI) from aqueous solution using modified corn stalks: Characteristic, equilibrium, kinetic and thermodynamic study. *Chemical Engineering Journal*, **168**(2), 909-917.

Dong, X., Ma, L.Q., Li, Y. 2011a. Characteristics and mechanisms of hexavalent chromium removal by biochar from sugar beet tailing. *J Hazard Mater*, **190**(1-3), 909-15.

Dong, X., Ma, L.Q., Li, Y. 2011b. Characteristics and mechanisms of hexavalent chromium removal by biochar from sugar beet tailing. *Journal of Hazardous Materials*, **190**(1-3), 909-915.

Gao, Y., Yue, Q., Gao, B., Sun, Y., Wang, W., Li, Q., Wang, Y. 2013. Comparisons of

porous, surface chemistry and adsorption properties of carbon derived from Enteromorpha prolifera activated by H4P2O7 and KOH. *Chemical Engineering Journal*, **232**, 582-590.

Guan, Q., Gao, K., Ning, P., Miao, R., He, L. 2020. Value-added utilization of paper sludge: Preparing activated carbon for efficient adsorption of Cr(VI) and further hydrogenation of furfural. *ence of The Total Environment*, **741**, 140265.

Jiang, X., Xiang, X., Hu, H., Meng, X., Hou, L. 2018. Facile Fabrication of Biochar/Al 2 O 3 Adsorbent and Its Application for Fluoride Removal from Aqueous Solution. *Journal of Chemical & Engineering Data*.

Jiang, Y., Li, F., Ding, G., Chen, Y., Liu, Y., Hong, Y., Liu, P., Qi, X., Ni, L. 2015. Synthesis of a novel ionic liquid modified copolymer hydrogel and its rapid removal of Cr (VI) from aqueous solution. *Journal of Colloid and Interface Science*, **455**, 125-133.

Kong, L.L., Liu, W.T., Zhou, Q.X. 2014. Biochar: An Effective Amendment for Remediating Contaminated Soil.

Li, J., He, F., Shen, X., Hu, D., Huang, Q. 2020. Pyrolyzed fabrication of N/P co-doped biochars from (NH4)(3)PO4-pretreated coffee shells and appraisement for remedying aqueous Cr(VI) contaminants. *Bioresource Technology*, **315**.

Li, Y., Gao, B., Wu, T., Sun, D., Li, X., Wang, B., Lu, F. 2009. Hexavalent chromium removal from aqueous solution by adsorption on aluminum magnesium mixed hydroxide. *Water Research*, **43**(12), 3067-3075.

Liang, H., Song, B., Peng, P., Jiao, G., Yan, X., She, D. 2020. Preparation of three-dimensional honeycomb carbon materials and their adsorption of Cr(VI) (vol 367, pg 9, 2019). *Chemical Engineering Journal*, **387**.

Liu, H., Liang, S., Gao, J., Huu Hao, N., Guo, W., Guo, Z., Wang, J., Li, Y. 2014. Enhancement of Cr(VI) removal by modifying activated carbon developed from Zizania

caduciflora with tartaric acid during phosphoric acid activation. *Chemical Engineering Journal*, **246**, 168-174.

Liu, Y., Xu, H. 2007. Equilibrium, thermodynamics and mechanisms of Ni2+ biosorption by aerobic granules. *Biochemical Engineering Journal*, **35**(2), 174-182.

Mahdavi, S., Jalali, M., Afkhami, A. 2013. HEAVY METALS REMOVAL FROM AQUEOUS SOLUTIONS USING TiO2, MgO, AND Al2O3 NANOPARTICLES. *Chemical Engineering Communications*.

Onchoke, K.K., Sasu, S.A. 2016. Determination of Hexavalent Chromium (Cr(VI)) Concentrations via Ion Chromatography and UV-Vis Spectrophotometry in Samples Collected from Nacogdoches Wastewater Treatment Plant, East Texas (USA). *Advances in Environmental Chemistry*, **2016**, 1-10.

Petkovska, Menka. 2014. Discrimination between adsorption isotherm models based on nonlinear frequency response results. *Adsorption-journal of the International Adsorption Society*, **20**(2-3), 385-395.

Ramavandi, B., Asgari, G., Faradmal, J., Sahebi, S., Roshani, B. 2014. Abatement of Cr (VI) from wastewater using a new adsorbent, cantaloupe peel: Taguchi L16 orthogonal array optimization. *Korean Journal of Chemical Engineering*, **31**(12), 2207-2214.

Rathinam, Karthik, Sankaran, Meenakshi. 2014. Facile synthesis of cross linked-chitosan–grafted-polyaniline composite and its Cr(VI) uptake studies. *International Journal of Biological Macromolecules*.

Santiago, M., Santhamani, S., Gilkes, R.J., Prakongkep, N. 2010. Remediation of chromium contaminated soils: potential for phyto and bioremediation. *World Congress of Soil Science: Soil Solutions for A Changing World*.

Sigmund, G., Hüffer, T., Kah, M., Hofmann, T. 2017. Effect of degassing temperature

558 on specific surface area and pore volume measurements of biochar. *Egu General Assembly*
559 *Conference*.
560 Singh, G., Lakhi, K.S., Sil, S., Bhosale, S.V., Kim, I.Y., Albahily, K., Vinu, A. 2019.
561 Biomass derived porous carbon for CO 2 capture. *Carbon*, **148**, 164-186.
562 Sophia, C.A., Lima, E.C. 2018. Removal of emerging contaminants from the
563 environment by adsorption. *Ecotoxicology & Environmental Safety*, **150**(APR.), 1-17.
564 Suganya, S., Kumar, P.S. 2018. Influence of ultrasonic waves on preparation of active
565 carbon from coffee waste for the reclamation of effluents containing Cr(VI) ions. *Journal*
566 *of Industrial and Engineering Chemistry*, **60**, 418-430.
567 Tong, Y., Mcnamara, P.J., Mayer, B.K. 2019. Adsorption of organic micropollutants
568 onto biochar: a review of relevant kinetics, mechanisms and equilibrium. *Environmental*
569 *ence: Water Research & Technology*.
570 Wang, Y. 2018. Characteristics of biochars from different sources and their removal
571 mechanism of heavy metal ions, Shanghai Jiaotong University.
572 Xin, Zhang, Weijing, Fu, Yuanxue, Yin, Zhihua, Chen, Rongliang, Qiu. 2018.
573 Adsorption-reduction removal of Cr(VI) by tobacco petiole pyrolytic biochar: Batch
574 experiment, kinetic and mechanism studies. *Bioresource Technology*.
575 Xu, Q., Chen, Z., Wu, Z., Xu, F., Yang, D., He, Q., Li, G., Chen, Y. 2019a. Novel
576 lanthanum doped biochars derived from lignocellulosic wastes for efficient phosphate
577 removal and regeneration. *Bioresource Technology*, **289**.
578 Xu, X., Huang, H., Zhang, Y., Xu, Z., Cao, X. 2019b. Biochar as both electron donor
579 and electron shuttle for the reduction transformation of Cr(VI) during its sorption.
580 *Environmental Pollution*, **244**(JAN.), 423-430.
581 Yin, W., Guo, Z., Zhao, C., Xu, J. 2019. Removal of Cr(VI) from aqueous media by

582 biochar derived from mixture biomass precursors of Acorus calamus Linn. and feather
583 waste. *Journal of Analytical and Applied Pyrolysis*, **140**, 86-92.
584 Yu, Y., An, Q., Jin, L., Luo, N., Li, Z., Jiang, J. 2020. Unraveling sorption of Cr (VI)
585 from aqueous solution by FeCl3 and ZnCl2-modified corn stalks biochar: Implicit
586 mechanism and application. *Bioresource Technology*, **297**.
587 Zhang, B., Luan, L., Gao, R., Li, F., Li, Y., Wu, T. 2017. Rapid and effective removal
588 of Cr(VI) from aqueous solution using exfoliated LDH nanosheets. *Colloids and Surfaces*
589 *a-Physicochemical and Engineering Aspects*, **520**, 399-408.
590 Zhang, J., Zheng, P. 2015. A preliminary investigation of the mechanism of
591 hexavalent chromium removal by corn-bran residue and derived chars. *Rsc Advances*,
592 **5**(23), 17768-17774.
593 Zhao, N., Zhao, C., Lv, Y., Zhang, W., Du, Y., Hao, Z., Zhang, J. 2017. Adsorption
594 and coadsorption mechanisms of Cr(VI) and organic contaminants on H 3 PO 4 treated
595 biochar. *Chemosphere*, **186**(nov.), 422-429.
596 Zhou, L., Liu, Y., Liu, S., Yin, Y., Zeng, G., Tan, X., Hu, X., Hu, X., Jiang, L., Ding, Y.
597 2016a. Investigation of the adsorption-reduction mechanisms of hexavalent chromium by
598 ramie biochars of different pyrolytic temperatures. *Bioresource Technology*, **218**, 351-359.
599 Zhou, L., Liu, Y., Liu, S., Yin, Y., Zeng, G., Tan, X., Hu, X., Hu, X., Jiang, L., Ding,
600 Y., Liu, S., Huang, X. 2016b. Investigation of the adsorption-reduction mechanisms of
601 hexavalent chromium by ramie biochars of different pyrolytic temperatures. *Bioresource*
602 *Technology*, **218**, 351-359.
603

Figures

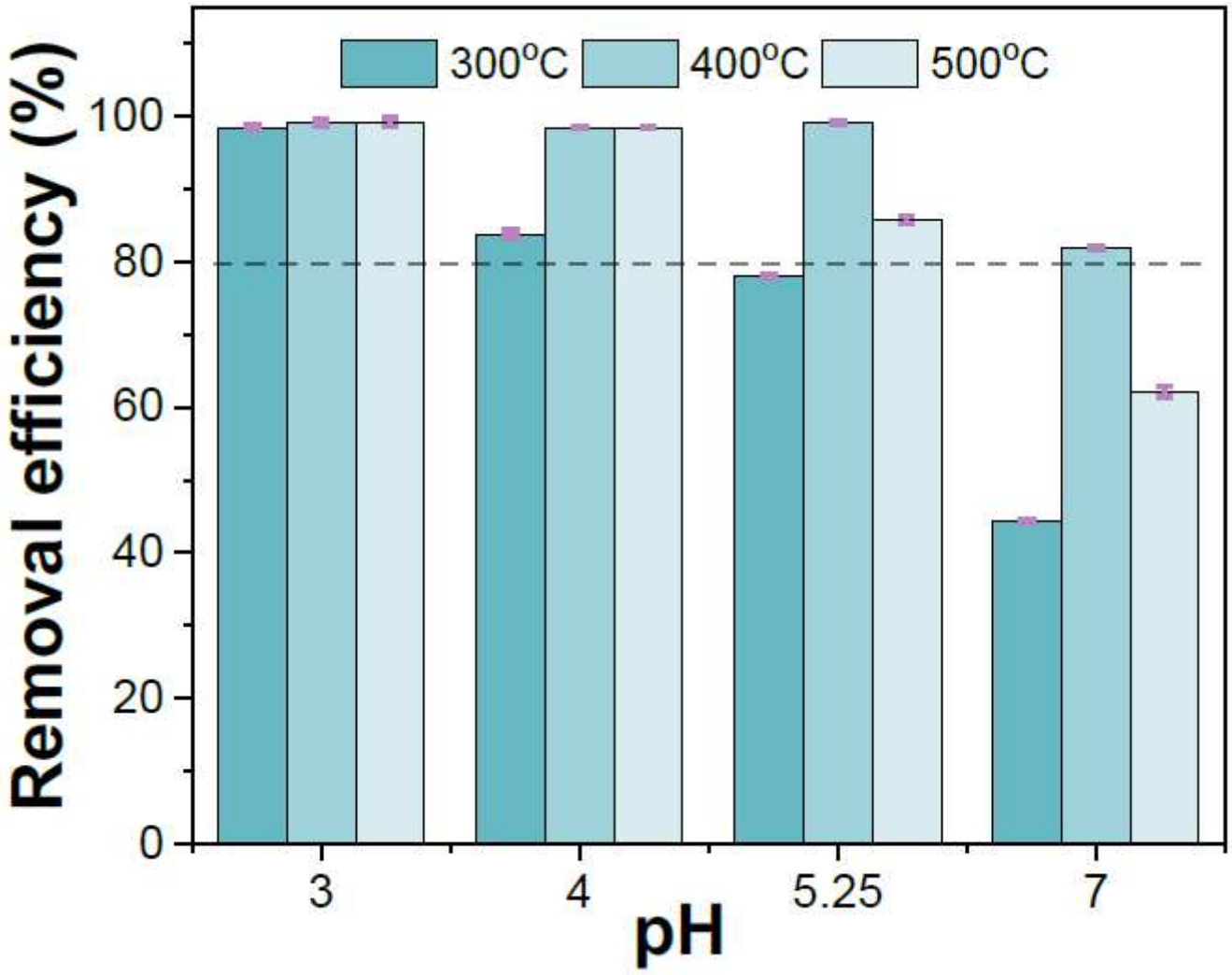

Figure 1

Cr(VI) removal efficiency at three activation temperatures. (Initial concentrations = 50 mg/L, Solution pH 5.25, and T=25°C).

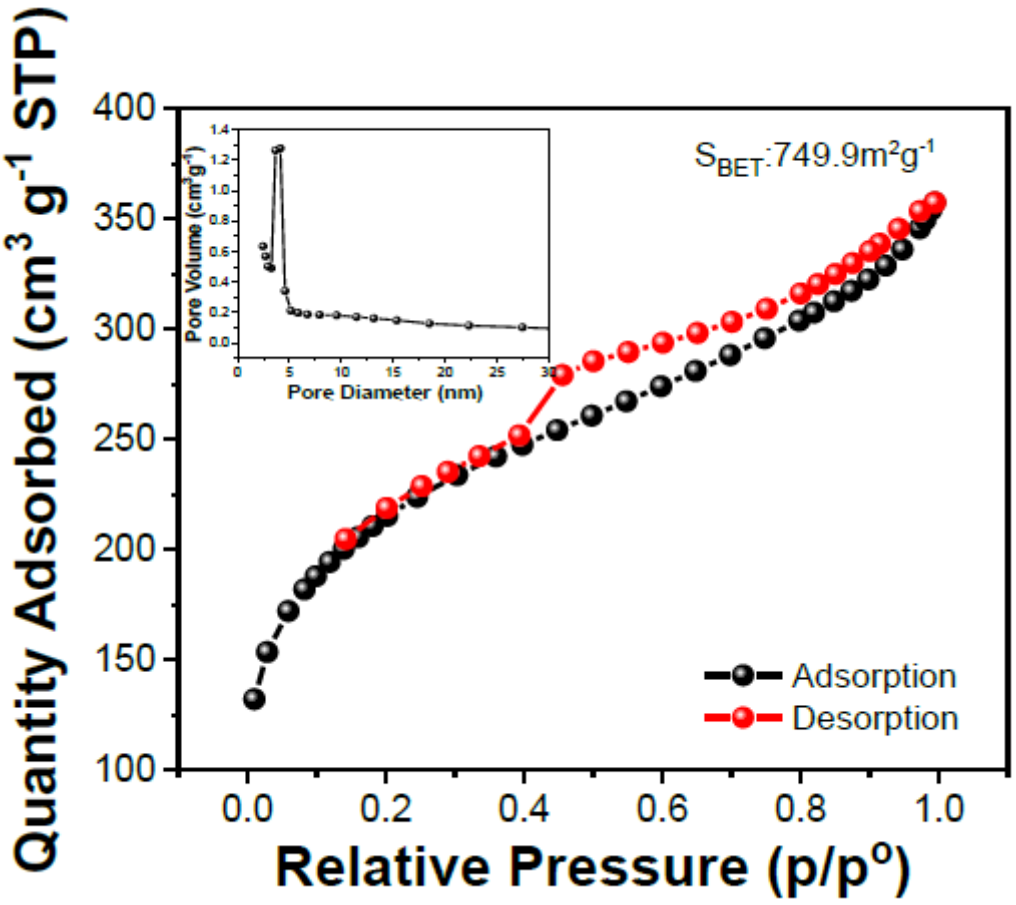

Figure 2

N2 adsorption/desorption isotherms and pore size distribution curve of Zp-pgBC-400°C.

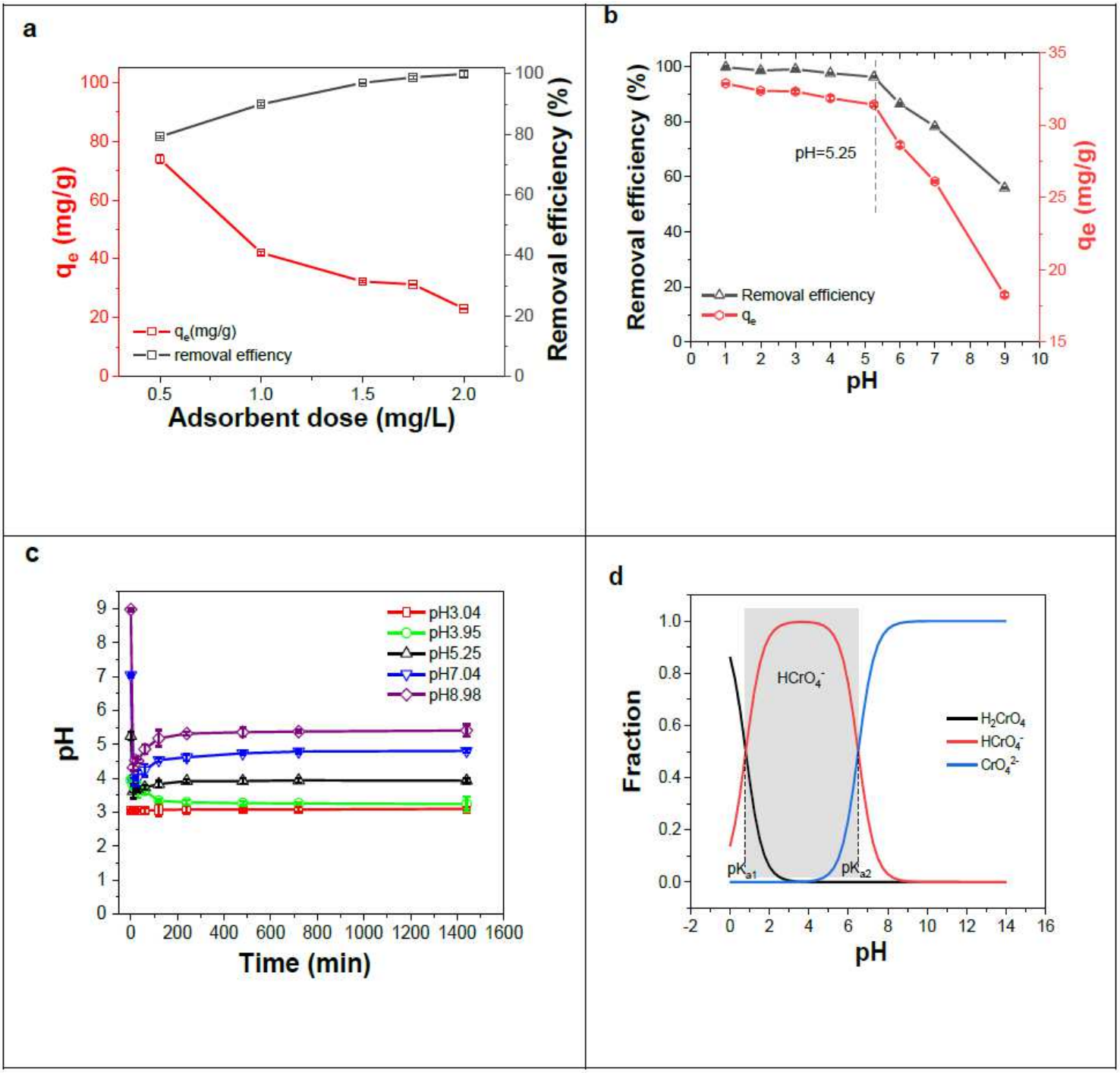

Figure 3

Effect of dosage (a) and solution pH (b) on Cr(VI) removal; (c)pH changing trend during reaction under various initial pH (5.25 was the intrinsic pH of the solution). T=298 K, C0(VI)=50 mg/g, rpm=160

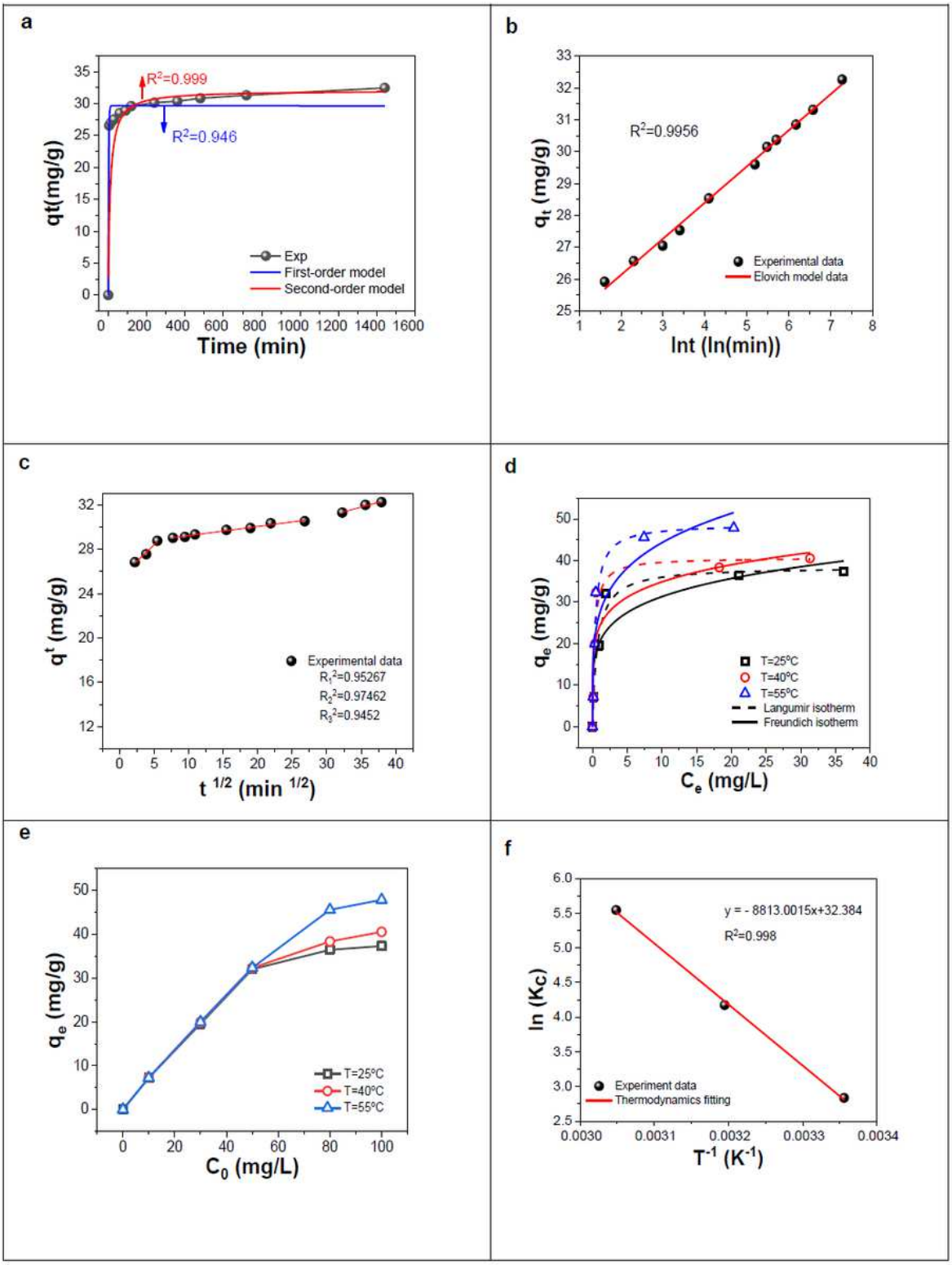

Figure 4

(a) Pseudo-first order and and Pesudo-second order; (b) Elovich model; (c) Intra-partice diffusion kinetic model; (d) Langmuir and Freundich adsorption isotherms; (e) Effects of original concentration on adsorption capacity at different temperature;(f)Thermodynamic plot solution pH 5.25, mass of adsorbent=1.5 g/L, and T=25°C).

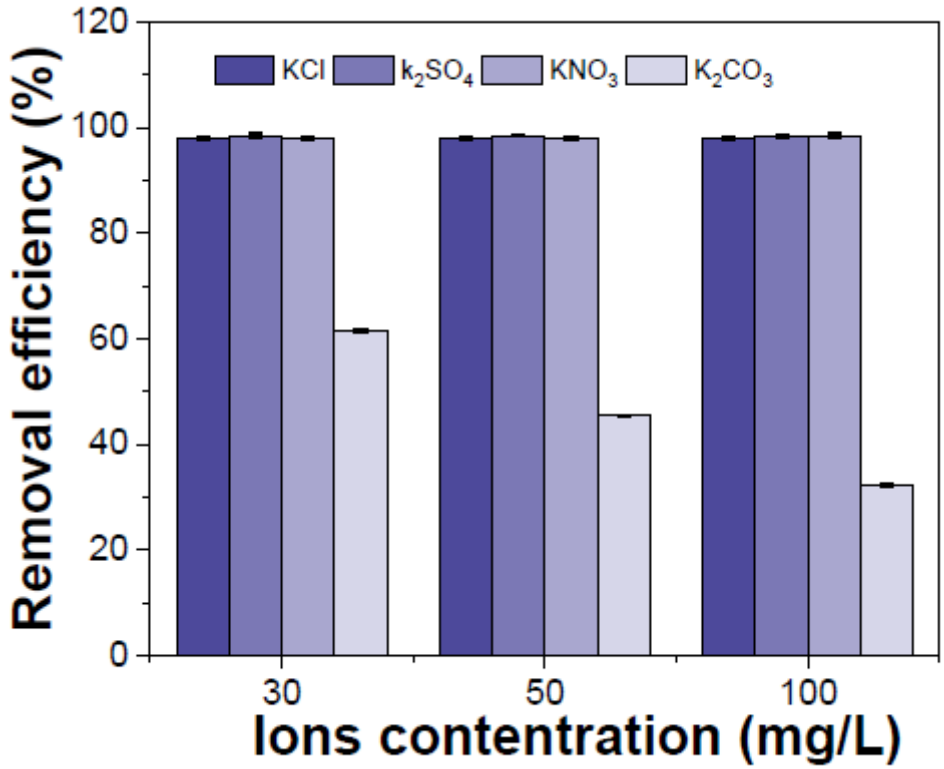

Figure 5

Effect of four common co-existing ions on Cr(VI) removal efficiency

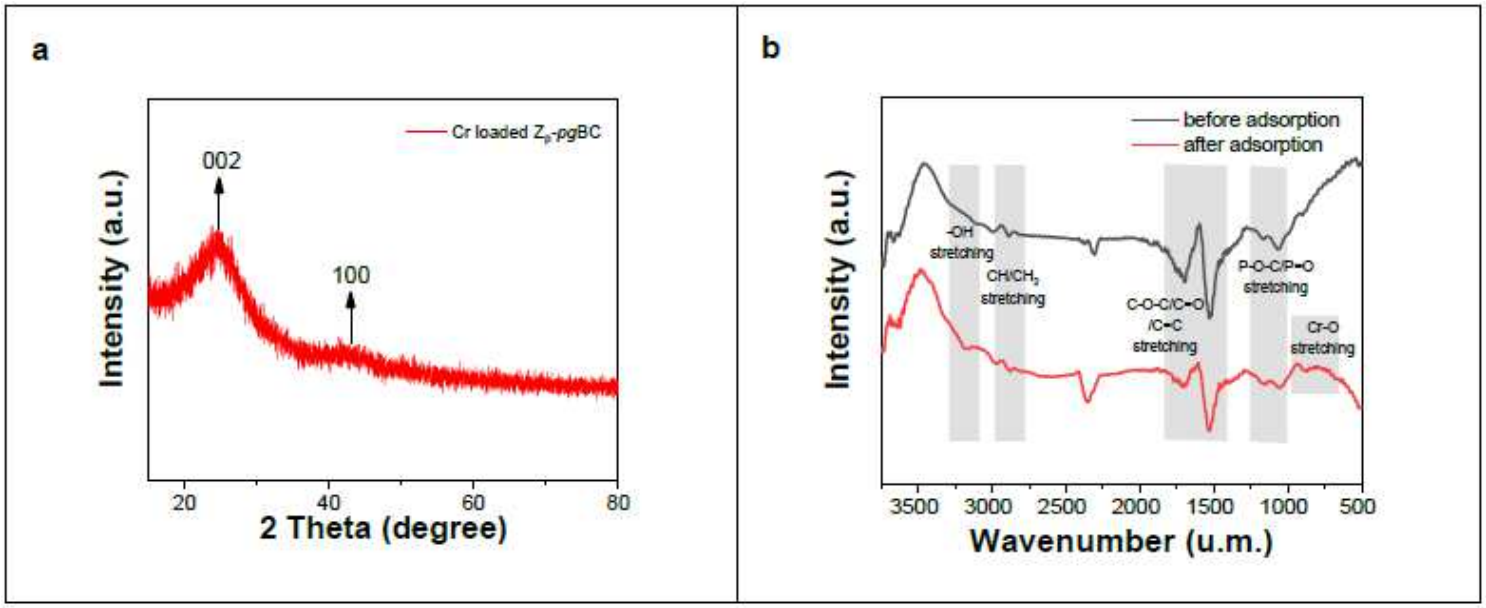

Figure 6

(a) XRD patterns, (b) FTIR spectra of Zp-pgBC-400°C.

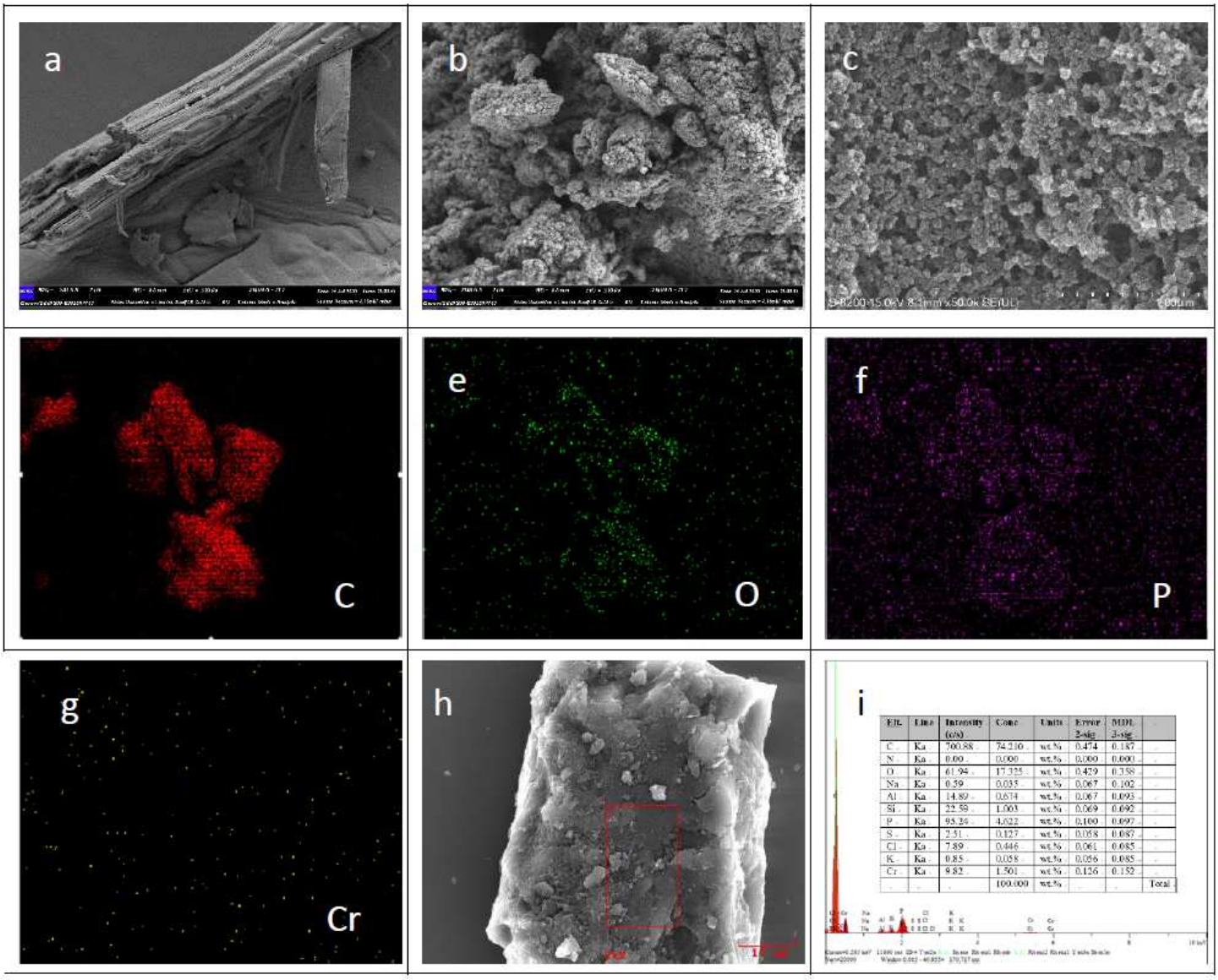

Figure 7

SEM images of Pennisetum giganteum (a); Zp-pgBC-400°C before (b) and after (c) Cr adsorption; Elemental mapping of (d) C, (e) O, (f) P, (g) Cr; (h) EDS point scan analysis area and (j) the corresponding EDS patterns.

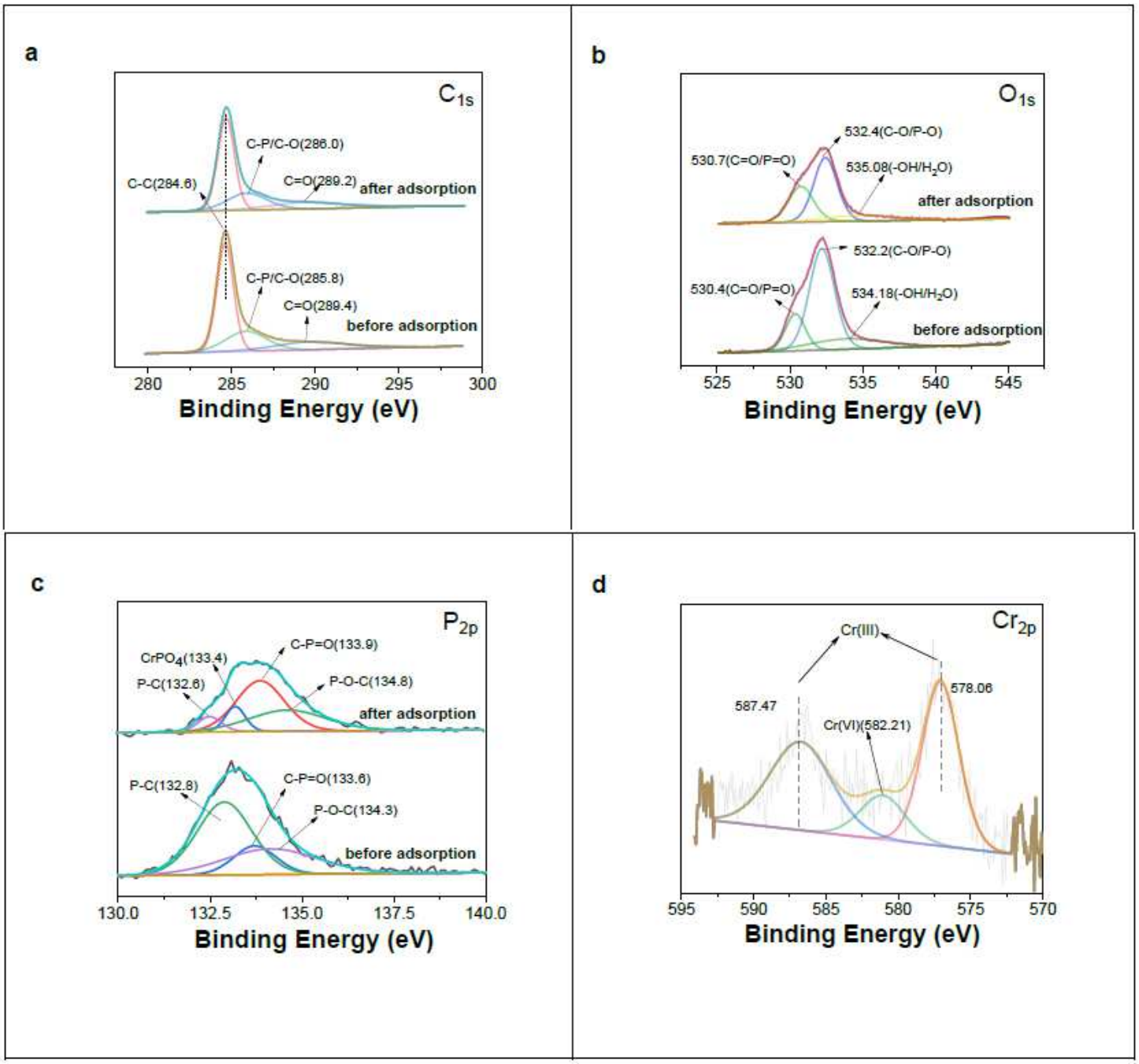

Figure 8

XPS spectrum of Zp-pgBC-400°C before and after Cr(VI) adsorption. (a) C1s, (b) O1s and (c) P2p and (d) Cr2p.

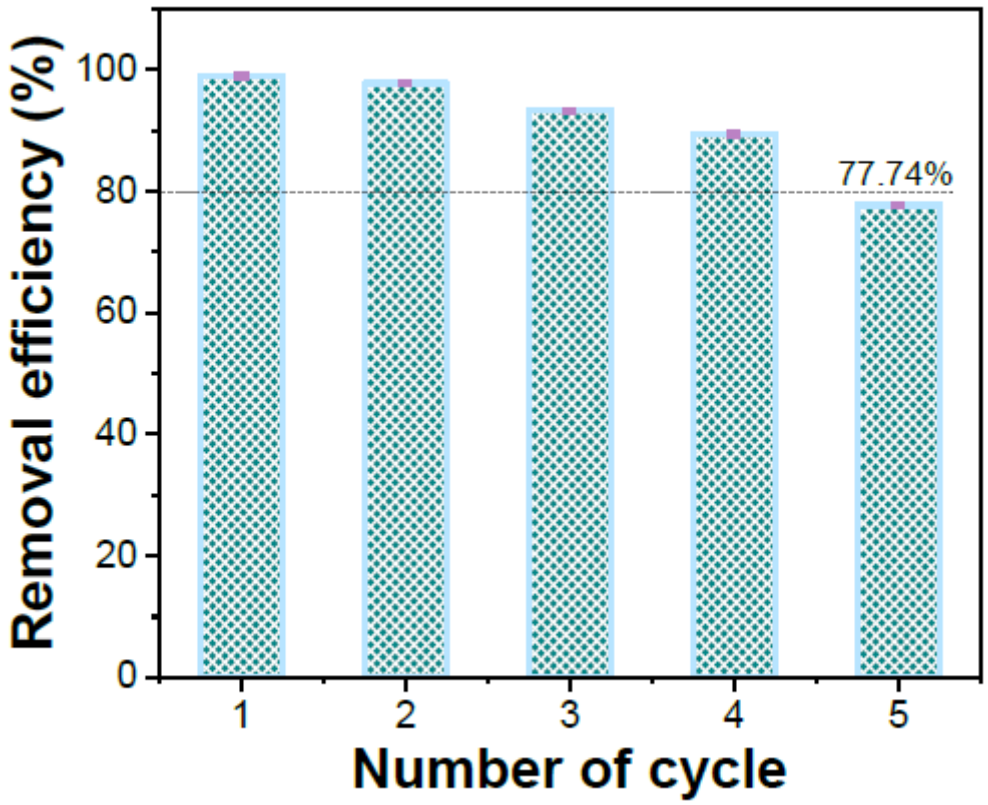

Figure 9

Cycle times of Zp-pgBC-400°C on Cr(VI) removal efficiency

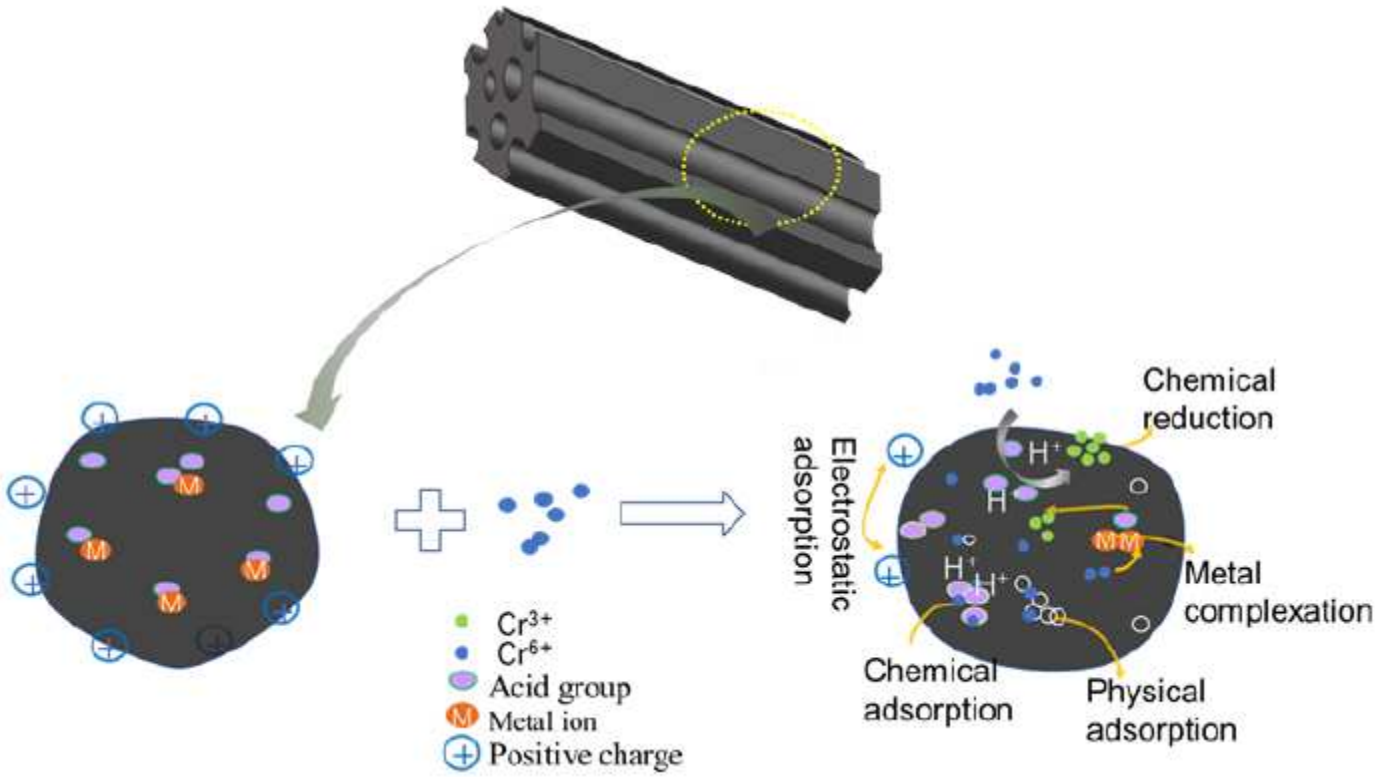

Figure 10

Schematic illustration of Cr(VI) removal mechanism

Supplementary Files

This is a list of supplementary files associated with this preprint. Click to download.

- GraphicalAbstract.png
- supportinformation.docx